Heliyon 8 (2022) e12079

Contents lists available at ScienceDirect

Heliyon

journal homepage: www.cell.com/heliyon

Research article

Entropy generation and characteristics of mixed convection in lid-driven trapezoidal tilted enclosure filled with nanofluid

Md. Shahneoug Shuvo, Mahmudul Hasan Hasib, Sumon Saha *

Department of Mechanical Engineering, Bangladesh University of Engineering and Technology, Dhaka 1000, Bangladesh

ARTICLE INFO

Keywords:
Nanofluid
Richardson number
Laminar flow
Mixed convection
Trapezoidal enclosure

ABSTRACT

The investigation of steady, incompressible, laminar mixed convective fluid flow within two different types of tilted lid-driven trapezoidal enclosures filled with nanofluid composed of water and Al_2O_3 nanoparticles has been carried out in this paper. The upper wall of the enclosure is an isothermal cold surface that travels at a constant speed, while the bottom surface of the cavity maintains a constant high temperature. Non-dimensional governing equations along with the appropriate boundary conditions are solved using Galerkin finite element technique. Parametric simulation has been conducted by varying tilt angle of the base wall from 0° to 45°, Reynolds number from 0.1 to 10^3, Grashof number from 10^{-2} to 10^6, and Richardson number between 0.1 and 10 for three different cases. The streamlines and the isotherms are used to describe the fluid flow and heat transfer characteristics within the enclosure. Besides, the quantitative evaluations of thermal enhancement in terms of the average Nusselt number, average fluid temperature, and Bejan number of the enclosure are presented. Effects of base wall tilt angle and the presence of nanofluid on convection heat transmission characteristics as well as Bejan number are also explored.

1. Introduction

Forced convection is always accompanied by natural convection, but in the case of considerably higher forced flow, the effect of forced convection gets dominated to such an extent that ignoring the buoyancy effect leaves very negligible error. On the other hand, in the case of extremely low fluid velocities, the opposite happens, that is natural convection gets dominated and thus cannot be neglected. Both natural and forced convection must be considered when velocity is such that the important governing parameter called Richardson number (Ri) is within the range of $0.1 \leq Ri \leq 10$. Several notable uses of mixed convection within a lid-driven enclosure include lubricating technologies, heating and drying technologies, and electronic device cooling, float glass production, food processing. Crystal growth, nuclear reactor thermo-hydraulics, metal plating, lake dynamics, reservoirs, cooling ponds, and other processing of materials are only a few examples of the applications of the research that has been done in this field.

During the assessment of Navier-Stokes solutions, Schreiber and Keller [1], Thompson and Ferziger [2] employed lid-driven cavity problems as a benchmark configuration to compare the numerical results. The diverse flow spectrum resulting from the interaction between forced flow and buoyancy effect within lid-driven trapezoidal enclosures offers a fascinating arena of mixed convection to investigate in-depth as well.

Numerous investigations on mixed convective flow in lid-driven enclosures have been conducted during the previous decades. Alleborn et al. [3] examined a numerical evaluation of mixed convection in a narrow container with a moving cold lid at the top and a hot lid at the bottom. In their research, they discovered that velocity parameters and the cavity length had an impact on mass and heat transfer. Additionally, they found two turning locations and flow designs that minimized heat and mass transfer. Khanafer and Chamkha [4] investigated numerically convective flow in a lid-driven square enclosure inside fluid-saturated porous material and examined the influence of Richardson and Darcy numbers on heat transmission characteristics of the enclosure. Using a square cavity, Yang and Aydin [5] numerically investigated mixed convection heat transfer for the discrete heat source. They examined the impact of Richardson number and heat source length on fluid flow and heat transfer. Javed et al. [6] investigated the effects of varying the heating conditions on the behavior of mixed convection flow within a lid-driven trapezoidal cavity. They found that changing the lid motion had no effect when the Rayleigh number was at 10^5. Bakar et al. [7]

* Corresponding author.
E-mail address: sumonsaha@me.buet.ac.bd (S. Saha).

https://doi.org/10.1016/j.heliyon.2022.e12079
Received 26 May 2022; Received in revised form 3 August 2022; Accepted 25 November 2022

Table 1. A summary of prior research on mixed convection in a trapezoid chamber.

Authors	Method	Fluid	*Re*	*Gr*	*Ri*	θ	γ
Mamun et al. [17]	FVM	Air	400, 600	1.6×10^4–3.6×10^6	0.1–10	30°–60°	30°–60°
Bhattacharya et al. [18]	FEM	Liquid metal, air, water	1, 100	1–10^4	1	0°	45°
Hasib et al. [19]	FEM	Al_2O_3-water	50	2.5×10^3	1	0°–45°	15°
Aghaei et al. [20]	FVM	Cu-water	30–1000	90–10^7	0.1–10	0°	15°–60°
Kareem et al. [21]	FVM	Al_2O_3-, CuO-, SiO_2-, TiO_2-water	100–1200	10^3–1.44×10^7	0.1–10	30°–60°	30°–60°
Arefmanesh et al. [22]	FVM	Cu-water	10–10^3	10^4	0.01, 0.1, 1, 100	0°	45°
Selimefendigil et al. [23]	FEM	Al_2O_3-water	44–1414	10^5	0.05–50	0°	0°–20°
Selimefendigil and Oztop [24]	FEM	Al_2O_3-water	63–1414	10^5	0.05–25	0°	15°, 22.5°
Toghraie and Davood [25]	FVM	Cu-water	-	-	0.1–1	0°	0°–40°
Ibrahim and Hirpho [26]	FEM	Water	100	10^3–10^5	0.1, 1, 10	0°	45°
Shah et al. [27]	FEM	Air	300–500	9×10^3–2.5×10^6	0.01–10	0°	15°
Mondal and Mahapatra [28]	FDM	Al_2O_3-water	10–100	10^3–10^6	0.01–100	0°	45°–90°
Ishak et al. [29]	FEM	Al_2O_3-water	5–500	0.25–2.5×10^6	0.01–10	0°	15°

investigated mixed convection within a lid-driven cavity while employing an inclined magnetic field. They demonstrated that the presence of the magnetic field slowed down the flow of mixed convection. Recently, Xiong et al. [8] investigated the effects of various configurations of the obstacles on the mixed convection flow within the lid-driven triangular chamber. They discovered that the Richardson number was a progressively increasing function of the Nusselt number.

Nanoparticles (often less than 100 nm in size) are distributed in a plain fluid such as ethylene glycol, water, or propylene glycol to produce a nanofluid with a solid volume fraction of less than 0–5%. Utilizing high metallic nanoparticles having higher thermal conductivity such as silver, copper, silicon, or aluminum in the composition enhances the thermal conductivity of that nanofluid with its increasing total energy transfer capabilities [9]. Nanofluid is a commonly used fluid that has improved heat and mass transfer properties in recent developments. Its applications include heat radiators, buildings cooling, plants, vehicular cooling, and so on. The use of nanofluid enhances heat transmission, reduces the size of heat transfer systems, minimizes blockage, cools microfluidic devices, and compacts systems [10].

Talebi et al. [11] utilized a Cu-water nanofluid flow in a square chamber that was lid-driven. They employed the finite volume method (FVM) and observed that the nanoparticle percentage had significant impacts on thermal behavior and flow pattern for a certain Reynolds number (*Re*). By utilizing the finite volume approach along with the SIMPLER algorithm, Mahmoodi [12] explored heat transmission and mixed convection fluid flow in rectangular enclosures driven by the bottom wall and filled with Al_2O_3-water nanofluid. He found that a main counterclockwise vortex formed within the domain at low Richardson numbers. Mansour et al. [13] carried out the numerical modeling of mixed convective flow in a square lid-driven reservoir that was partly heated from below and filled with nanofluid. The finite difference method (FDM) was used to discretize the governing equations of their problem [13]. They noticed that although the fluid activity and temperature were reduced, an increase in the percentage of solid volume led to an increase in the average Nusselt number. The finite element method (FEM) was utilized by Rahman et al. [14] to study heat transfer enhancement in a triangular lid-driven inclined enclosure filled with nanofluid. At three different convective regimes, they discovered that the nanoparticle percentage had a significant impact on heat transmission and fluid flow in the enclosure. Ismael et al. [15] studied mixed convection in a cavity with a moving lid and hybrid nanofluid inside it. Their results showed that the hybrid nanofluid strategy had a good chance of making things more economic by decreasing the number of expensive nanoparticles with high thermal conductivity. Mixed convection in a double lid-driven rectangular chamber filled with hybrid nanofluids was studied by Ali et al. [16]. They found that particle-fluid interaction had a significant impact on convective heat transmission rates.

Many studies have focused on basic geometric shapes such as rectangle, square, and triangle for the design of the enclosure. However, the real enclosures that are used in practice are typically different from the basic shapes in terms of their design. Irregular shapes may be found in a variety of building materials, electrical panels, and solar energy collectors. It is also worth noting that just a few prior research has looked at the trapezoidal geometry, which is used in numerous practical applications. Mixed convection inside trapezoidal enclosure has a substantial impact on the interior temperature and flow profiles. Hence, extensive investigation on trapezoidal enclosure is required to build more effective heating and cooling systems in future. Only a few investigations in past focused on mixed convective flow in a lid-driven trapezoidal chamber [17, 18, 19, 20, 21, 22, 23, 24, 25, 26, 27, 28, 29]. All those studies along with geometric conditions (e.g., sidewall inclination angle, γ and tilt angle, θ), working fluids, governing parameters (e.g., *Ri*, *Re* and Grashof number, *Gr*) and numerical methods are summarized in Table 1.

Furthermore, a review report by Izadi et al. [30] revealed that only around 3% of the research had been conducted on trapezoidal shape cavities filled with Cu-water or Al_2O_3-water nanofluids being the most prevalent nanofluids in this field of study. Another review article by Mustafa et al. [31] concluded that when the angle of inclination of the cavity increased, heat transmission levels decreased. They further noted that mixed convection was inferior to forced convection in terms of fluid flow and heat transfer.

Following a review of the previous similar studies as listed in Table 1, it is fair to conclude that Mamun et al. [17], Hasib et al. [19], and Kareem et al. [21] conducted investigations in a tilted lid-driven trapezoidal enclosure. However, no entropy generation analysis has been done on the tilted trapezoidal enclosure in these works along with the systematic presentation of the influence of mixed convection governing parameters under different cases. This research aims to investigate the presence of nanofluid and tilt angle on entropy formation and heat transmission in lid-driven two symmetrical trapezoidal enclosures. The findings are shown in the form of parametric presentations of isotherms and streamlines for different mixed convection cases. Furthermore, the impacts of different governing parameters and base wall inclination angles on the heat transmission process are quantitatively investigated, and the findings of this study are reported in terms of average Nusselt number at the bottom heated wall, average fluid temperature as well as Bejan number.

2. Problem definition

Two isosceles trapezoidal enclosures with one having a longer hot wall at a temperature, T_h and the other with a shorter hot wall maintaining the same temperature are considered in the present study (see Figs. 1(a) and (b), respectively), with an aspect ratio of $L/H = 1.268$ and 0.732 respectively. Both enclosures have insulated sidewalls with an inclination angle of $\gamma = 15°$. Allowing the top cold wall at a temperature T_c to move with a fixed speed U_0, the remaining walls are kept stationary. The hot base wall is assumed to be tilted at an angle of 0°, 30°, and 45° with respect to the horizontal direction, respectively. Assume that the nanofluid (Al_2O_3-water) within the trapezoid is

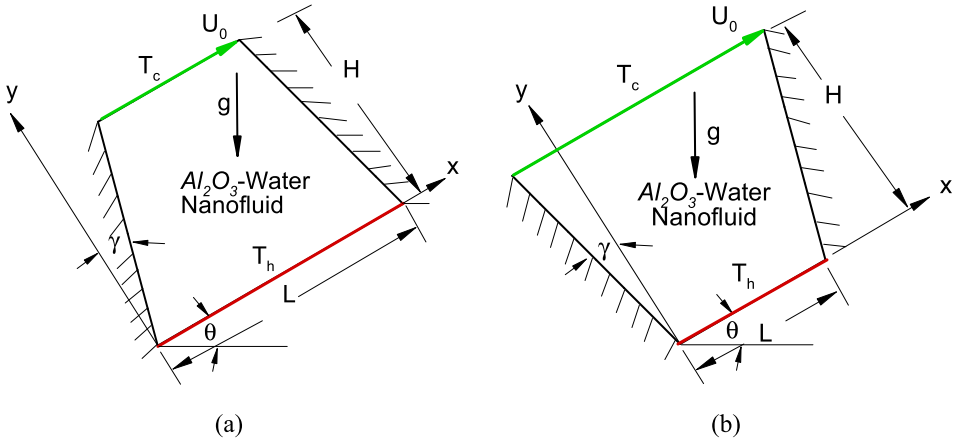

Fig. 1. Schematic diagram of the computational domains with (a) longer base trapezoid and (b) shorter base trapezoid.

incompressible and Newtonian with constant thermos-physical properties. Besides, the Boussinesq approximation is used to approximate the temperature field, which relates temperature changes as a function of fluid density. The analysis ignores viscous dissipation, radiation, and internal heat generation.

The mathematical model for governing steady laminar, mixed convection utilizing conservation of mass (1), momentum (2)–(3) and thermal energy (4) can be formulated in the following way [19]:

$$\frac{\partial U}{\partial X}+\frac{\partial V}{\partial Y}=0, \tag{1}$$

$$U\frac{\partial U}{\partial X}+V\frac{\partial U}{\partial Y}=-\frac{\partial P}{\partial X}+\frac{\mu_{nf}\rho_f}{\mu_f\rho_{nf}}\frac{1}{Re}\left(\frac{\partial^2 U}{\partial X^2}+\frac{\partial^2 U}{\partial Y^2}\right)+\frac{\beta_{nf}}{\beta_f}(Ri\sin\theta)\Theta, \tag{2}$$

$$U\frac{\partial V}{\partial X}+V\frac{\partial V}{\partial Y}=-\frac{\partial P}{\partial Y}+\frac{\mu_{nf}\rho_f}{\mu_f\rho_{nf}}\frac{1}{Re}\left(\frac{\partial^2 V}{\partial X^2}+\frac{\partial^2 V}{\partial Y^2}\right)+\frac{\beta_{nf}}{\beta_f}(Ri\cos\theta)\Theta, \tag{3}$$

$$U\frac{\partial \Theta}{\partial X}+V\frac{\partial \Theta}{\partial Y}=\frac{\alpha_{nf}}{\alpha_f}\frac{1}{RePr}\left(\frac{\partial^2 \Theta}{\partial X^2}+\frac{\partial^2 \Theta}{\partial Y^2}\right), \tag{4}$$

The dimensionless scales (5) used in the above equations have the following definitions [19]:

$$X=\frac{x}{H},\quad Y=\frac{y}{H},\quad U=\frac{u}{U_0},\quad V=\frac{v}{U_0},\quad P=\frac{p}{\rho_{nf}U_0^2},\quad \Theta=\frac{T-T_c}{T_h-T_c}, \tag{5}$$

where, U and V stand for non-dimensional velocity components as per Cartesian coordinate system X and Y respectively. Non-dimensional temperature is expressed by Θ and non-dimensional pressure is expressed by P. Similarly, the related dimensional quantities are expressed by u, v, T and p respectively. Reynolds number, Grashof number, Richardson number, and Prandtl number (Pr) are the non-dimensional governing parameters appeared respectively, which are defined by the following relations (6) as:

$$Re=\frac{\rho_f U_0 H}{\mu_f},\quad Gr=\frac{\rho_f^2 g\beta_f\left(T_h-T_c\right)H^3}{\mu_f^2},\quad Ri=\frac{Gr}{Re^2},\quad Pr=\frac{\mu_f C_{p,f}}{k_f}. \tag{6}$$

The following relationships (7)–(10) can be used to determine the thermos-physical properties of the nanofluid (Al_2O_3-water) using mixing law theory [29],

Mass density:

$$\rho_{nf}=(1-\phi)\rho_f+\phi\rho_s, \tag{7}$$

Heat capacity:

$$\left(\rho C_p\right)_{nf}=(1-\phi)\left(\rho C_p\right)_f+\phi\left(\rho C_p\right)_s, \tag{8}$$

Table 2. Thermo-physical properties of water, Al_2O_3 nanoparticles and water-Al_2O_3 nanofluid.

Physical properties	Plain Fluid (water, $\phi=0$)	Solid phase (Al_2O_3)	Al_2O_3-water nanofluid ($\phi=0.01$)
C_p (J/kg K)	4179	765	4047
k (W/m K)	0.613	25	0.64306
ρ (kg/m^3)	997.1	3970	1026.8
$\beta\times10^5$ (1/K)	21	0.85	20.51
μ (Pa.s)	0.001003	-	0.001093
α (m^2/s)	1.471×10^{-7}	8.232×10^{-6}	1.548×10^{-7}
Pr	6.4348	-	6.8788

Table 3. Non-dimensional boundary conditions used in the current study.

Boundary	Thermal Condition	Velocity Condition
Bottom wall	$\Theta=1$	$U=0$, $V=0$
Top wall	$\Theta=0$	$U=1$, $V=0$
Side walls	$\partial\Theta/\partial N=0$	$U=0$, $V=0$

Thermal expansion coefficient:

$$(\rho\beta)_{nf}=(1-\phi)(\rho\beta)_f+\phi(\rho\beta)_s, \tag{9}$$

Thermal diffusivity:

$$\alpha_{nf}=\frac{k_{nf}}{\left(\rho C_p\right)_{nf}}. \tag{10}$$

Azmi et al. [32] computed the thermal conductivity and viscosity of a mixture of a plain fluid and a diluted suspension of small spherical particles which can be calculated as (11)–(12):

$$k_{nf}=0.8938(1+\phi)^{1.37}\left(1+\frac{T-273}{70}\right)^{0.2777}\left(1+\frac{d_s}{170}\right)^{-0.0336}\times\left(\frac{\alpha_s}{\alpha_f}\right)^{0.01737}k_f, \tag{11}$$

$$\mu_{nf}=\mu_f(1+\phi)^{11.3}\left(1+\frac{T-273}{70}\right)^{-0.038}\left(1+\frac{d_s}{170}\right)^{-0.061}, \tag{12}$$

where, d_s (= 47 nm) is the diameter of Al_2O_3 nanoparticles and T (K) is the temperature of Al_2O_3-water nanofluid, ϕ denotes the volume fraction of Al_2O_3 nanoparticles. Symbols with subscripts 'nf', 'f', and 's' denote properties of nanofluid (Al_2O_3-water), base fluid (water) and solid particles (Al_2O_3). Table 2 lists the thermo-physical properties of water ($\phi=0$), Al_2O_3 nanoparticles and water-Al_2O_3 nanofluid ($\phi=0.01$) at $T=313$ K [4]. Table 3 presents the non-dimensional boundary conditions for this problem, where N denotes distance normal to the boundary.

The average fluid temperature (Θ_{av}) inside the enclosure (13) and the average Nusselt number (Nu) of the bottom heated wall (14) can be defined according to [19] as follows:

$$\Theta_{av} = \frac{1}{A}\int_A \Theta dA, \tag{13}$$

$$Nu = -\frac{k_{nf}}{k_f}\frac{H}{L}\int_0^{L/H} \left.\frac{\partial \Theta}{\partial Y}\right|_{Y=0} dX, \tag{14}$$

where, A is the non-dimensional area of the enclosure. The mixed convective flow domain generates entropy primarily via heat transfer ($S_{l,h}$) and the viscous effects of the fluid ($S_{l,f}$). These can be defined in non-dimensional forms (15)–(16) referencing to [29],

$$S_{l,h} = \frac{k_{nf}}{k_f}\left[\left(\frac{\partial \Theta}{\partial X}\right)^2 + \left(\frac{\partial \Theta}{\partial Y}\right)^2\right], \tag{15}$$

$$S_{l,f} = \varphi\frac{\mu_{nf}}{\mu_f}\left[2\left(\frac{\partial U}{\partial X}\right)^2 + 2\left(\frac{\partial V}{\partial Y}\right)^2 + \left(\frac{\partial U}{\partial Y} + \frac{\partial V}{\partial X}\right)^2\right], \tag{16}$$

where irreversibility distribution ratio (φ) is defined as (17):

$$\varphi = \frac{\mu_f (T_h + T_c)}{2k_f}\left(\frac{U_0}{T_h - T_c}\right)^2. \tag{17}$$

By integrating the local values throughout the whole domain, it is possible to deduce average entropy production as follows (18):

$$S_h = \frac{1}{A}\iint_A S_{l,h} dA, S_f = \frac{1}{A}\iint_A S_{l,f} dA. \tag{18}$$

A further major irreversibility variable known as the Bejan number is designated to show how much irreversibility is made through heat transfer compared to how much entropy is made overall [29]. The definition of average Bejan number is as follows (19):

$$Be = \frac{S_h}{S_h + S_f}. \tag{19}$$

3. Numerical procedure

The governing equations are discretized using the Galerkin finite element method together with the required boundary conditions (see Table 3), and then the numerical solutions are performed using the commercial CFD tool "COMSOL Multiphysics 6.0." Zienkiewicz and Taylor [33] provided extensive documentation on the implementation of this approach. The non-linear parametric computational approach is used to determine the governing equations' numerical solution. Compared to previous approaches, this one ensures convergence much more quickly. A triangular non-uniform mesh arrangement (free mesh) is used in the current simulation to obtain quick changes in the unknown variables, principally close to the lower hot wall. Six nodding triangular elements are also utilized since it is useful for them to detect nonlinear changes of field variable smoothly. Following that, a system of integral equations is constructed using the Galerkin weighted residual method utilizing the nonlinear governing partial differential equations. The Gauss quadrature method must be used to integrate each term of these equations. On the algebraic nonlinear equations, boundary conditions are then imposed. The nonlinear equations are solved repeatedly using the Broyden's technique in conjunction with a LU-decomposition preconditioner utilizing the LU-decomposition method. For the error criteria, a relative tolerance of 10^{-6} is taken into account. Manual scaling of the unknown variables is done to improve computational convergence because the magnitudes of the dependent variables vary greatly. The manual scaling values are retained fixed and picked in such a way that, when used, the scaled degrees of freedom have magnitudes of one.

Table 4. Grid independence study in terms of average Nusselt number at heated base wall of the trapezoidal enclosure for $\theta = 45°$, $Re = 100$, $Gr = 10^5$ and $\phi = 0.01$.

Element number	Longer base trapezoid	Element number	Shorter base trapezoid
993	3.9892	987	7.5429
1524	4.1260	1512	7.6489
2542	4.2147	2522	7.7058
6617	4.3890	6643	7.8872
17232	**4.4698**	**17180**	**7.9672**
26540	4.4672	26424	7.9653

3.1. Grid sensitivity check

A wide variety of mesh combinations has been investigated and reported in the current work, which covers six distinct non-uniform grid systems. Table 4 shows the outcomes of the investigation. Based on these comparisons, it is established that a total of 6617 and 6643 mesh elements is adequate to yield an acceptable result for longer and shorter base trapezoids respectively. However, to provide a better grid independent solution, a total of 17232 and 17180 elements for longer and shorter base trapezoids respectively has been selected for the current investigation.

3.2. Model verification

The computational algorithm is verified using findings from Bhattacharya et al. [18] for mixed convection flows in a trapezoidal enclosure and a square enclosure as presented by Roy et al. [34]. This is because validation with similar experimental results is not available. Fig. 2(a) illustrates the discrepancy of average Nusselt number at the lower heated wall of a trapezoidal enclosure having $\theta = 0°$ against Bhattacharya et al. [18], which is in excellent agreement. Another resemblance of the Bejan number inside the square enclosure using the current model with Roy et al. [34] at $Re = 1$ for water ($\phi = 0$) is conducted. The comparison is presented in Fig. 2 (b), and it is seen that the obtained data is in close harmony with Roy et al. [34]. Both comparisons provide a good agreement in terms of Nusselt number and Bejan number.

Furthermore, the resemblance of streamline and isotherms with Bhattacharya et al. [18] at $Re = 100$ and $Gr = 10^3$ are plotted in Figs. 3(a) and (b), respectively. Streamline and isotherm patterns show similar trends and values in comparison with those of Bhattacharya et al. [18]. The consistency observed in the Nusselt number, Bejan number, streamline, and isotherm plots verify the existing model and give a great deal of confidence in the execution of the further numerical simulation.

4. Results and discussion

Simulations have been carried out to study the steady, laminar, mixed convective flow inside trapezoidal enclosure provided with a sliding lid and a temperature gradient. When analyzing heat transfer in a lid-driven trapezoidal enclosure, Richardson number provides a measurement of the relative significance of natural convection over forced convection. In the case of $Ri = 1$, it defines a dominating mixed convection mode, whereas in the case of $Ri > 1$, it defines buoyancy-driven enclosure flow behavior for a non-stratified fluid [35, 36].

Different flow conditions are simulated by varying enclosure tilt angle and volume fraction of the solid particles under three different cases as listed in Table 5. Inclination angle is changed from 0° to 45°, and nanofluid with the volume fraction of 0% (water) and 1% (Al_2O_3-water) is considered in the present study to understand their effects on thermal and flow fields. The buoyancy force only impacts in the Y-direction for a horizontal cavity ($\theta = 0°$). Buoyancy forces act in both X- and Y-directions for inclined enclosures ($\theta = 30°$ and 45°). Effect on heat transfer characteristics has been explored in this study by describing average fluid temperature and average Nusselt number at the bottom

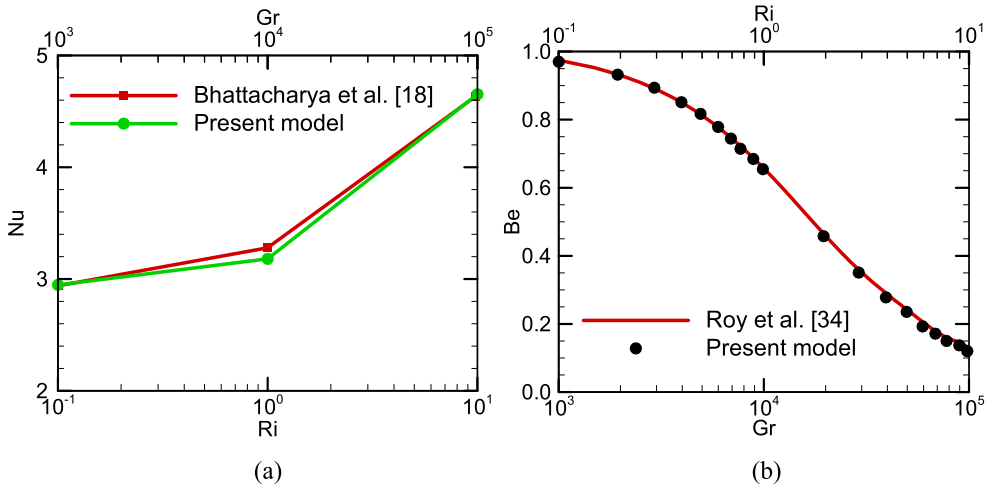

Fig. 2. Resemblance of (a) average Nusselt number at heated lower wall of the trapezoidal enclosure, and (b) Bejan number inside the square enclosure using the current model with Bhattacharya et al. [18] and Roy et al. [34] respectively computed at (a) $Re = 100$, $\theta = 0°$, $Pr = 10$ and (b) $Re = 1$, $Pr = 7.2$ respectively.

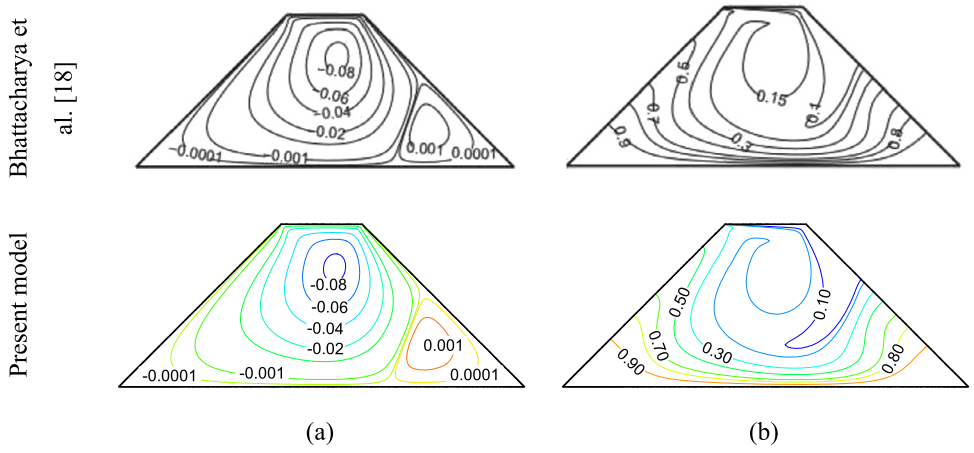

Fig. 3. Resemblance of (a) streamline, and (b) isotherm with Bhattacharya et al. [18] computed at $Re = 100$, $Gr = 10^3$, $\theta = 0°$, $Pr = 10$.

Table 5. Selection of governing and physical parameters for the current investigation.

Case	*Re*	*Gr*	*Ri*	θ	ϕ	φ
1	100	10^3–10^5	0.1–10	0°, 30°, 45°	0, 0.01	2.05×10^{-4}–2.05
2	31.62–316.22	10^4	0.1–10	0°, 30°, 45°	0, 0.01	2.05×10^{-3}–2.05×10^{-1}
3	0.1–10^3	10^{-2}–10^6	1	0°, 30°, 45°	0, 0.01	2.05×10^{-4}–2.05×10^{4}

heated wall of the enclosure in detail under both geometric configurations. Measurement of entropy generation in terms of Bejan number for both geometric configurations is also explored under these three different cases.

4.1. Effect of Ri and Gr at fixed value of Re

In case 1, Richardson number, which determines the order of effect encompassing both free convection and forced convection, has been varied within a range of 0.1 to 10 with varying Grashof number within a range of 10^3 to 10^5 for a fixed $Re = 100$. The results show that Richardson number has a significant effect on both natural and forced convection. As seen in Figs. 4(a)-(f) and 5(a)-(f), both flow and thermal fields vary with the variation of the parameters *Ri* and *Gr* simultaneously.

The forced flow induces at the right-moving upper wall and then descends until it reaches the bottom section. Upon reaching the lower zone, it begins to travel left, and upon reaching the bottom-left corner, it turns upwards. The shear effect dominates the buoyancy effect in the transition state of forced-mixed convection environment ($Ri = 0.1$). The moving lid supports to generate a main recirculation cell that covers most of the cavity with a secondary eddy on the right-bottom corner. Because the corner angle is bigger than the right angle, the secondary eddy is less in size the shorter base trapezoid. Specifically, for the pure mixed convection dominated environment ($Ri = 1$), the buoyancy impact and the shear effect owing to the sliding lid are both statistically significant. Streamlines depict two recirculating cells of varying diameters in this case. Fig. 4 shows a bigger eddy than the shorter base trapezoid (Fig. 5), which is located at the right-bottom corner. However, there are no secondary eddies in the shorter base trapezoid (right-bottom corner) as shown in Fig. 5. This is because primary vortices cover the whole enclosure due to the higher corner angle at the bottom of the enclosure compared to the longer base trapezoid. Besides, the longer top lid allows more circulating fluid to encounter the sliding motion resulting in the formation of only one main vortex inside the enclosure. A single main recirculation system is seen in shorter base trapezoid for $Ri = 0.1$ and 10. In the case of $Ri = 10$, when the flow is at the transition state of natural-mixed convection, the buoyancy effect is dominating. The secondary circulation is located at the top moving lid in all cases. With rising Richardson number, the flow field becomes

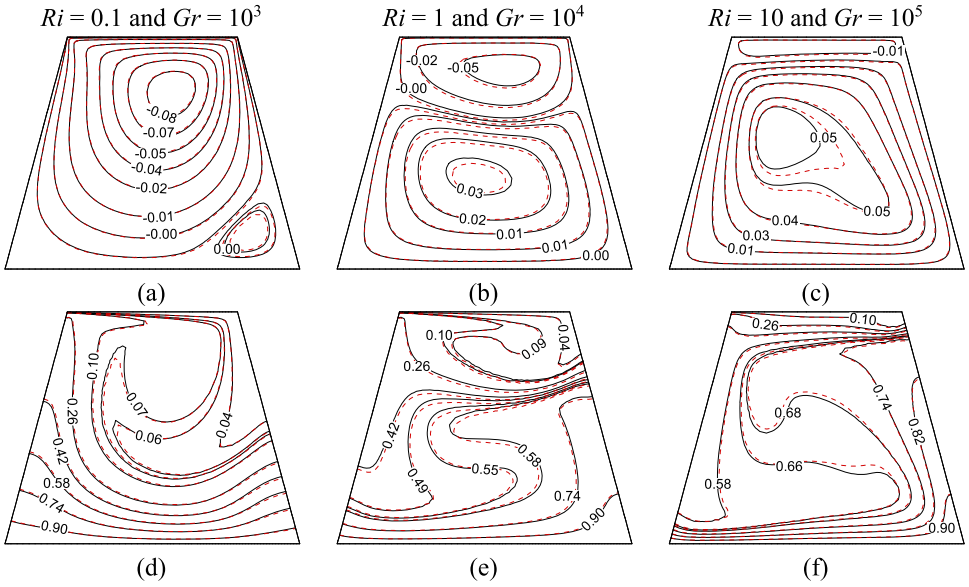

Fig. 4. Plots of (a)-(c) streamlines and (d)-(f) isotherms between nanofluid and plain fluid for different values of Ri and Gr at $\theta = 45°$, $Re = 100$ inside longer base trapezoidal enclosure. The solid lines (—) represent data for plain fluid, whereas the dotted lines (- - - -) represent the same for nanofluid.

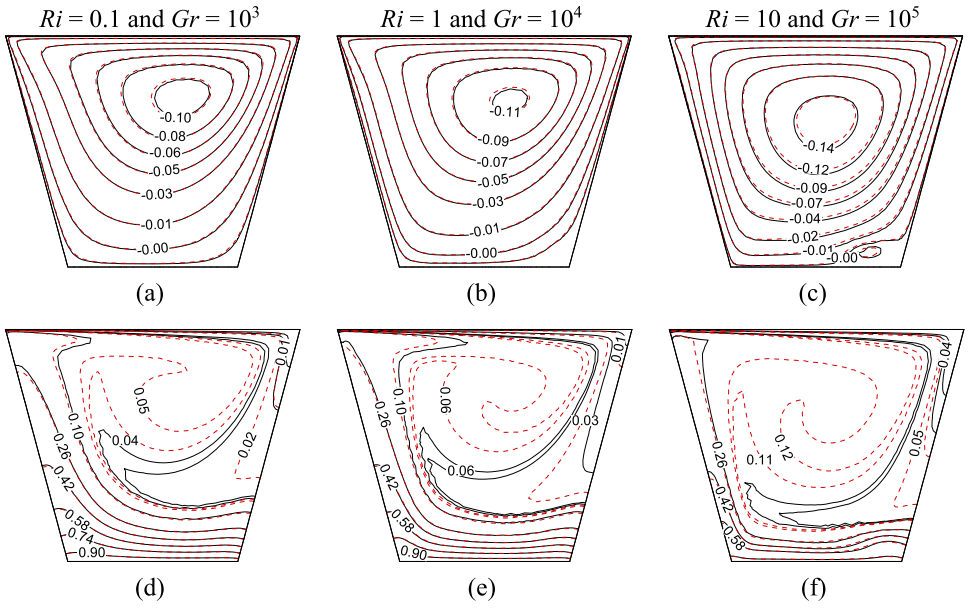

Fig. 5. Plots of (a)-(c) streamlines and (d)-(f) isotherms between nanofluid and plain fluid for different values of Ri and Gr at $\theta = 45°$, $Re = 100$ inside shorter base trapezoidal enclosure. The solid lines (—) represent data for plain fluid, whereas the dotted lines (- - - -) represent the same for nanofluid.

slower, and the center of the primary large vortex is pushed towards the center of the enclosure.

In addition, as shown in Figs. 4 and 5, certain significant variations in the isotherms are seen for different values of Richardson number. The isotherms also suggest a similar situation for the heat transmission characteristic inside the enclosure, which is consistent with the previous findings [30, 31]. As the value of Richardson number rises, the isotherms near the hot wall become stronger, and vice versa. In nature, the isotherms seem to be more uniform at first. When Richardson number is increased, the non-linearity of the isotherms rises at a higher value resulting in greater plume production, and the development of a deformed plume showing improved convective heat transfer for $Ri = 10$. Since the level of mechanical turbulence decreases with increasing Richardson number, the growth of the plume moves closer to neutral stability. This phenomenon can be visualized through isotherms.

When $Ri = 1$, buoyancy and shear effects are both at about the same level. As Ri goes up, natural convection dominates over mixed convection. However, for lower Ri, where most of the convection is dominated by forced flow, there is less heat transfer as shown in Figs. 6(a) and (b), respectively. Also, it is important to note that forced to natural convection dominance changes at $Ri = 0.8$ ($Gr = 8 \times 10^3$) and 3 ($Gr = 3 \times 10^4$) for horizontal ($\theta = 0°$) longer and shorter base trapezoids respectively. When trapezoids are tilted, this transition Richardson number is less than for horizontal trapezoids. However, it should be mentioned that the mechanism of mixed convection involves within the limiting range of $0.1 \leq Ri \leq 10$. The total heat transmission is decreased due to the inclination of the thermal line. On the other hand, nanofluid has considerable effect on temperature fields. Figs. 4 and 5 show shifting of isotherms for nanofluid which clearly denotes that nanofluid increases heat augmentation process for those trapezoids.

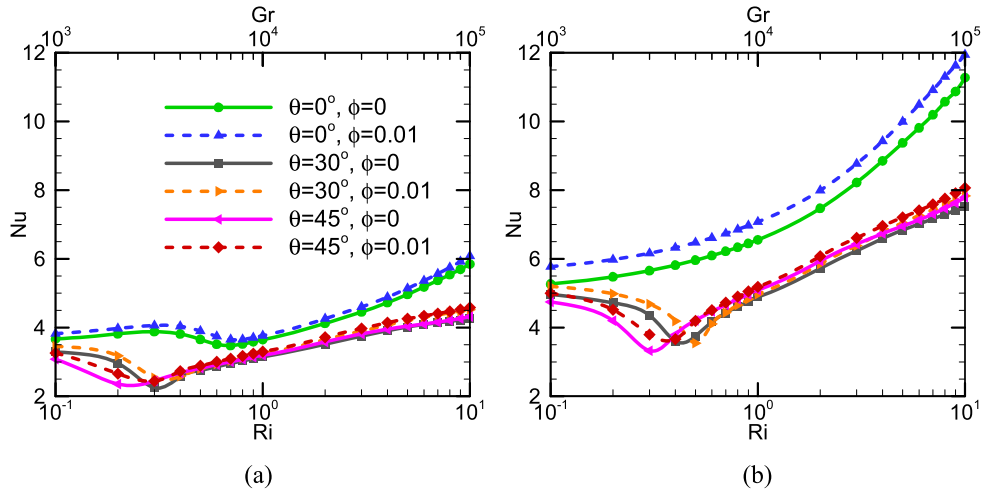

Fig. 6. Variation of average Nusselt number of the heated wall of (a) longer base trapezoid and (b) shorter base trapezoid with Richardson and Grashof numbers for different tilt angles in both plain and nanofluid at $Re = 100$.

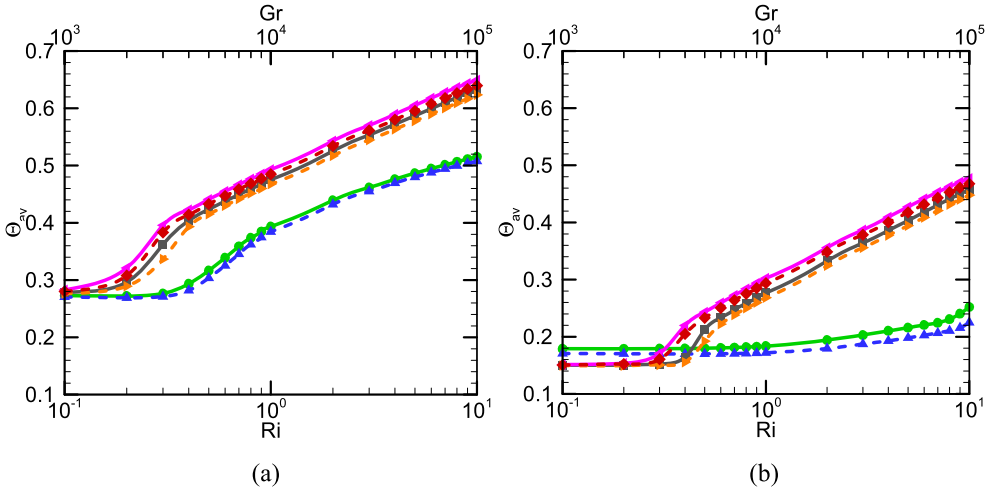

Fig. 7. Variation of average fluid temperature of (a) longer base trapezoid and (b) shorter base trapezoid with Richardson and Grashof numbers for different tilt angles in both plain and nanofluid at $Re = 100$. The datasets are the same as in Fig. 6(a).

The impact of the base wall tilt angle on changes in average Nusselt number and average fluid temperature of the enclosure with $Ri = 0.1$ to 10, and $\phi = 0$, 0.01 are plotted in Figs. 6(a)-(b) and 7(a)-(b) for $\theta = 0°$, 30° and 45°. Nusselt number lowers at first and then grows again where average fluid temperature rises sharply with Richardson number for both types of inclined enclosures. The average Nusselt number and average fluid temperature representing the amount of heat transferred are both improved by the presence of nanofluid. From Figs. 6 and 7, it can be deducted that larger Nusselt number and smaller average fluid temperature are found for shorter base trapezoid compared to the longer one. In both configurations, increasing the tilt angle reduces the average Nusselt number. The reason behind the reduction of Nu is that when the inclination angle increases, the hot surface is dominated by dead zones, which corresponds to a low-temperature gradient. Due to this, it is suggested that an inclination angle that is too high is not used for applications that need more heat transmission.

Effect of Richardson and Grashof numbers on average Bejan number is dictated in Figs. 8(a)-(b) with varying base wall tilt angle and volume percentage of nanoparticles at $Re = 100$. Here, average Bejan number is found to be increased by nanofluid. It is also found that average Bejan number gradually rises with increasing Ri and Gr. For all configurations, Be is much larger than 0.5 when $Ri > 0.5$. This leads to the conclusion that entropy development by heat transfer is much more dominant than that for viscous friction.

4.2. Effect of Ri and Re at fixed value of Gr

To visualize fluid flow and thermal fields, streamlines and isotherms are plotted in Figs. 9(a)-(f) and 10(a)-(f) for three different combinations of Ri and Re at fixed $\theta = 0°$ and $Gr = 10^4$ for longer and shorter base trapezoids respectively. For longer base trapezoid, the right vortex in the streamline plot tends to get occupied most of the enclosure as Ri increases and Re decreases, which indicates the dominance of natural convection over forced convection. However, for shorter base trapezoid, this effect is negligible since the fluid motion inside the enclosure is completely dominated by a circulating cell. For longer base trapezoids, the right vortex of the lines of flow tends to dominate as Ri increases and Re decreases at fixed Gr, which shows that natural convection is more dominant than forced convection. However, if the base is shorter, this effect is not high enough, because there is no such a vortex in the enclosure. On the other hand, for both enclosures, isotherms are seen dense at the lower heated wall indicating dominant conduction mode at lower Ri.

The average Nusselt number of the hot wall and average fluid temperature inside the enclosure are used to provide a quantitative mea-

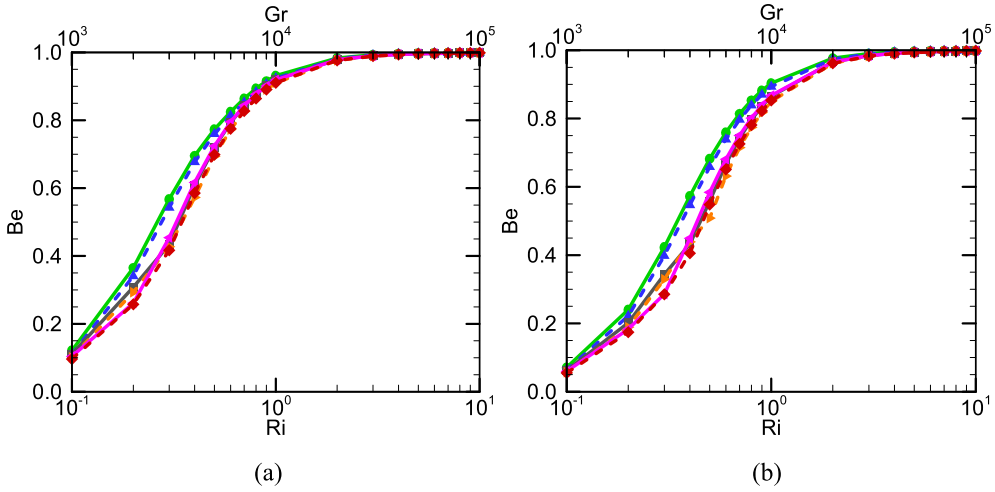

Fig. 8. Variation of average Bejan number of (a) longer base trapezoid and (b) shorter base trapezoid with Richardson and Grashof numbers for different tilt angles in both plain and nanofluid at $Re = 100$. The datasets are the same as in Fig. 6(a).

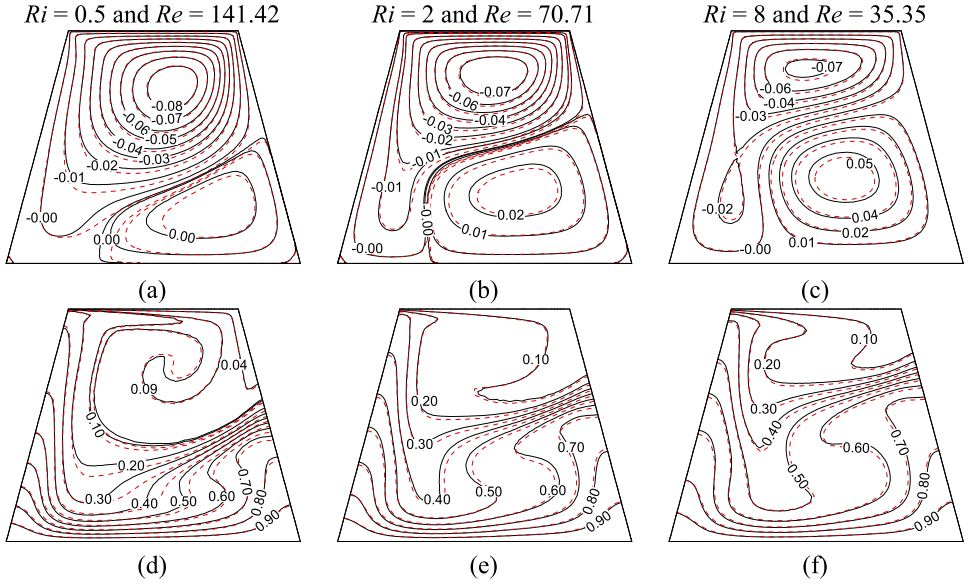

Fig. 9. Plots of (a)-(c) streamlines and (d)-(f) isotherms between nanofluid and plain fluid for different values of Ri and Re at $\theta = 0°$, $Gr = 10^4$ inside longer base trapezoidal enclosure. The solid lines (—) represent data for plain fluid, whereas the dotted lines (- - - -) represent the same for nanofluid.

surement of heat transfer performance with varying base wall tilt angles and nanoparticle volume percentages as illustrated in Figs. 11(a)-(b) and 12(a)-(b) respectively for different combinations of Re and Ri at $Gr = 10^4$. In the case of increasing Ri and decreasing Re at a given Gr, the Nusselt number falls. For longer base enclosure, this fall is quite quick at the beginning except $\theta = 45°$ and $\phi = 0$, and then it drops gradually with increasing Ri for all inclined enclosures. The Nusselt number also drops as the base wall tilt angle increases. The average fluid temperature in the enclosure rises as Ri grows (Re decreases), and it falls as Ri decreases. Moreover, it rises when the tilt angle of the base wall is increased. In fact, when the angle of inclination is increased, there is a reduction in the amount of buoyancy force that appeared in the body force term of momentum equations. As a result, the enclosure will have a higher average temperature. Nanofluid, on the other hand, causes improvement of both the average fluid temperature and the Nusselt number.

Figs. 13(a)-(b) shows the effect of Richardson and Grashof numbers on average Bejan number when the base wall tilt angle and volume percentage of nanoparticles are varied. Average Bejan number increases in proportion to the rise in Ri. When Ri is smaller and Re is larger, the Bejan number is greater than 0.5 indicating that heat transmission is the main force in entropy development. After raising Ri while simultaneously decreasing Re, this impact becomes far more dominating. Bejan number is seen to be one slowly for all combinations indicating that entropy growth happens solely during heat transfer and thus, there is no growth of viscous entropy generation. A drop in average Bejan number is also seen with an increase in overall entropy creation while using nanofluids. In case 2, the longer base trapezoid generates more total entropy than the shorter base trapezoid.

4.3. Effect of Re and Gr at fixed value of Ri

In this case, the impact of pure mixed convection ($Ri = 1$) for the various combinations of Re and Gr is identified. To distinguish laminar to chaotic regime, variation of average Nusselt number as a function of Re and Gr is presented in Figs. 14(a)-(b). Reynolds number is varied from 0.1 to 10^3 with the corresponding change of Grashof number from 0.01 to 10^6. Fig. 14 also illustrates the effect of volume percentage of nanoparticles ($\phi = 0$ and 0.01) on average Nusselt number. As expected, heat transmission increases with simultaneous rising of Re and Gr after

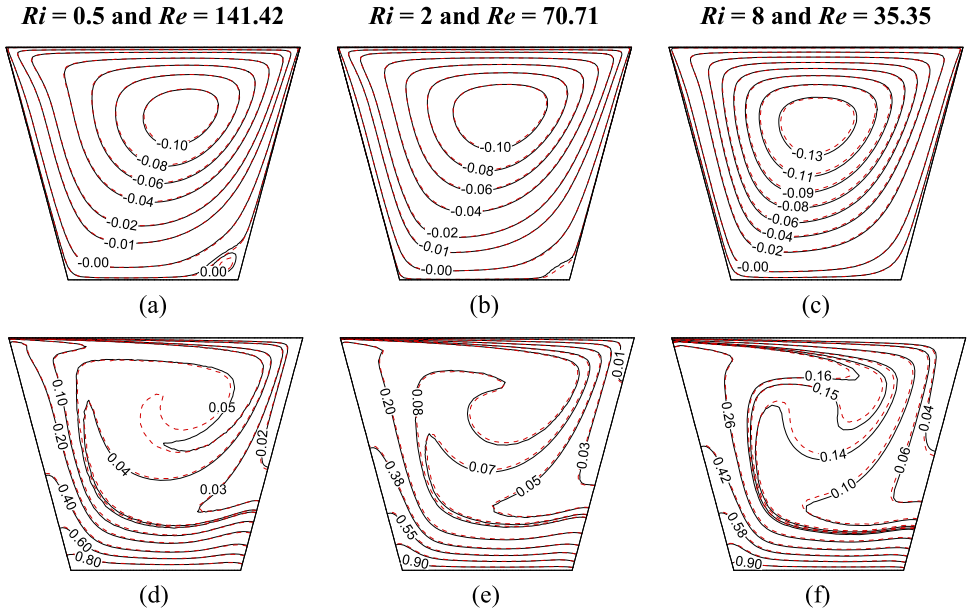

Fig. 10. Plots of (a)-(c) streamlines and (d)-(f) isotherms between nanofluid and plain fluid for different values of *Ri* and *Re* at $\theta = 0°$, $Gr = 10^4$ inside shorter base trapezoidal enclosure. The solid lines (—) represent data for plain fluid, whereas the dotted lines (- - - -) represent the same for nanofluid.

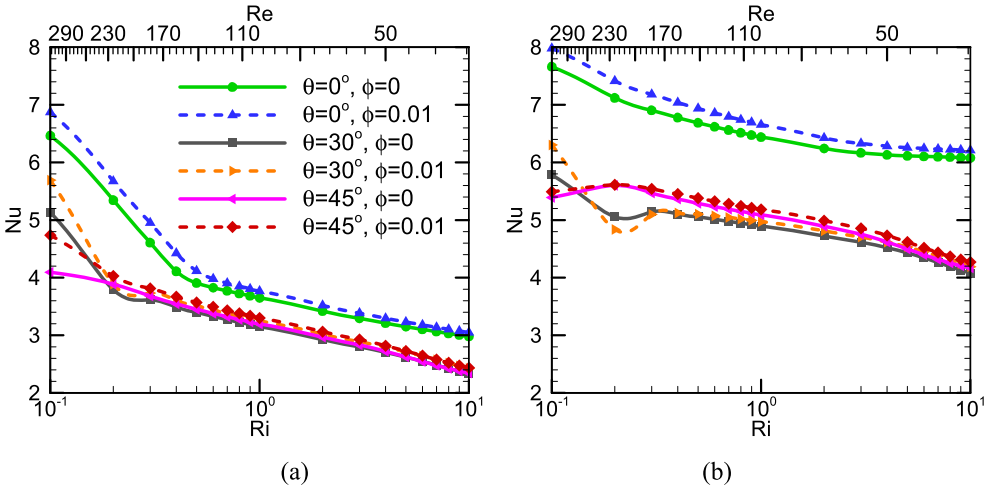

Fig. 11. Variation of average Nusselt number of the heated base wall of (a) longer base trapezoid and (b) shorter base trapezoid with Richardson and Reynolds numbers for different tilt angles in both plain and nanofluid at $Gr = 10^4$.

crossing the conduction dominated regime, where *Nu* is essentially constant. A typical transition state of laminar to chaotic regime for both types of enclosure is identified, where there is a sudden drop of *Nu* and then increasing sharping with increasing *Re* and *Gr*. This region is elaborately scrutinized through the visualization of streamline and isotherm plots as described next. Besides, the heat transmission rate of the heated bottom wall, i.e., Nusselt number is increased by the presence of nanofluid. However, the presence of nanoparticles has very little effect on this laminar to chaotic transition process as clearly visualized in the inset figures of Fig. 14.

To visualize laminar to chaotic transition qualitatively in pure mixed convection ($Ri = 1$), streamlines and isotherms are plotted for three combinations of *Re* and *Gr* as shown in Figs. 15(a)-(f) and 16(a)-(f) for larger and shorter base trapezoids respectively. It is clear to detect a little vortex in streamline ($Re = 37$ and $Gr = 1369$) at the right corner of longer base trapezoid. In a convection dominated mode, when laminar to chaotic transition takes place, that vortex seems to grow. A dense concentration of isotherms may also be seen along the hot wall for $Re = 37$ and $Gr = 1369$. Isotherms are spreading across the enclosure as *Re* and *Gr* grow. For higher *Re* and *Gr*, the shear and buoyancy effects dominate on both isotherms and streamlines.

As shown in Fig. 16 for streamline plots with a shorter base trapezoid, there is no vortex in the laminar regime. When the flow becomes chaotic, this right vortex begins to form and becomes dominant at greater *Re* and *Gr*. This is because with higher *Re* and *Gr* values, both forced and buoyancy driven forces are more prevalent. Moreover, it seems that isotherms are concentrated near heated walls at lower *Re* and *Gr*. When *Re* and *Gr* grow, isotherms spread out. Due to the geometry of the enclosure, the right vortex in a longer base trapezoid is greater than the same in a shorter base trapezoid. Having a wider base trapezoid allows this vortex to stretch out as well as to be more powerful. In both enclosures, isotherms seem to follow the same pattern, yet their values and shapes vary. In contrast, nanofluids have a considerable impact on flow patterns and temperature distributions. It seems that the vortex is becoming smaller, and the isotherms are being more evenly distributed for nanofluid indicating improved heat transfer.

Figs. 17(a)-(b) illustrate the variation of average Nusselt number as a function of *Re* and *Gr* at $Ri = 1$ and $\phi = 1\%$ for three values of tilt angle.

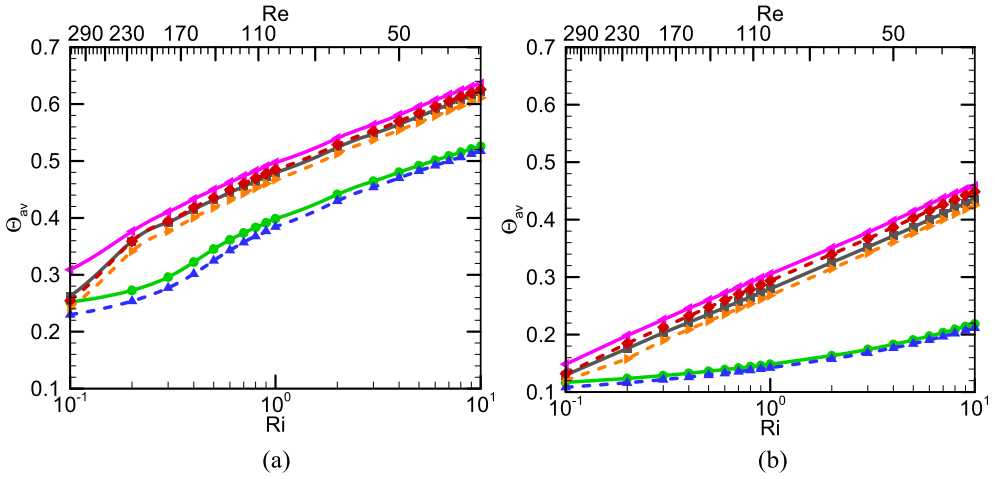

Fig. 12. Variation of average fluid temperature of (a) longer base trapezoid and (b) shorter base trapezoid with Richardson and Reynolds numbers for different tilt angles in both plain and nanofluid at $Gr = 10^4$. The datasets are the same as in Fig. 11(a).

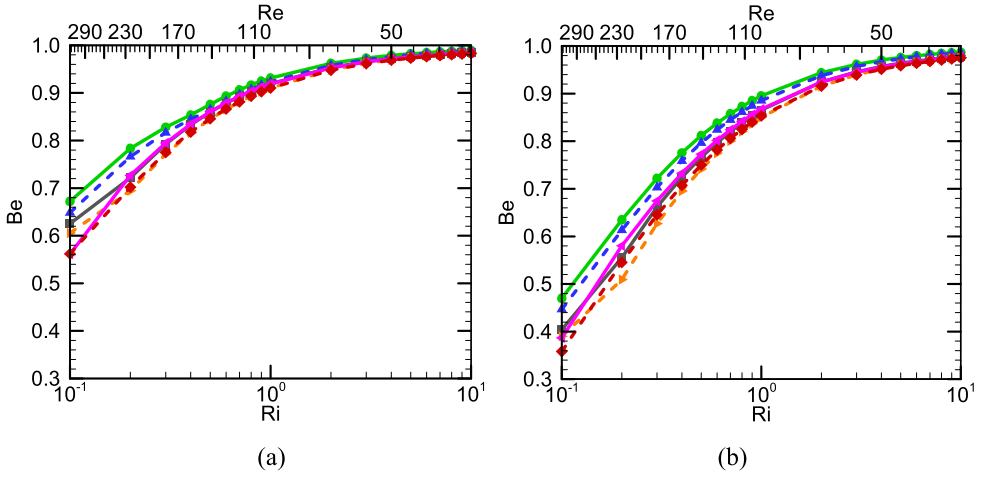

Fig. 13. Variation of average Bejan number of (a) longer base trapezoid and (b) shorter base trapezoid with Richardson and Reynolds numbers for different tilt angles in both plain and nanofluid at $Gr = 10^4$. The datasets are the same as in Fig. 11(a).

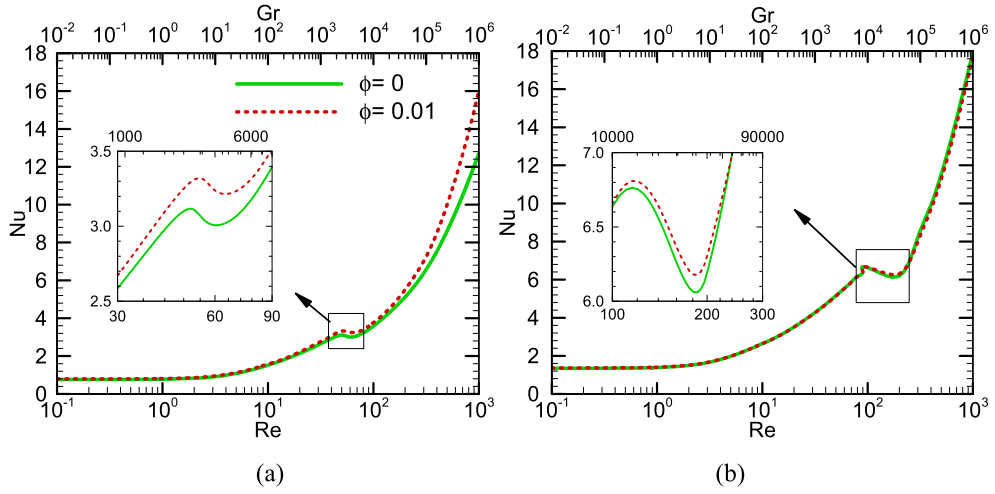

Fig. 14. Variation of average Nusselt number of the hot wall of (a) longer base trapezoid and (b) shorter base trapezoid with combined variation of *Gr* and *Re* for different nanoparticle solid volume fraction at $Ri = 1$ and $\theta = 0°$.

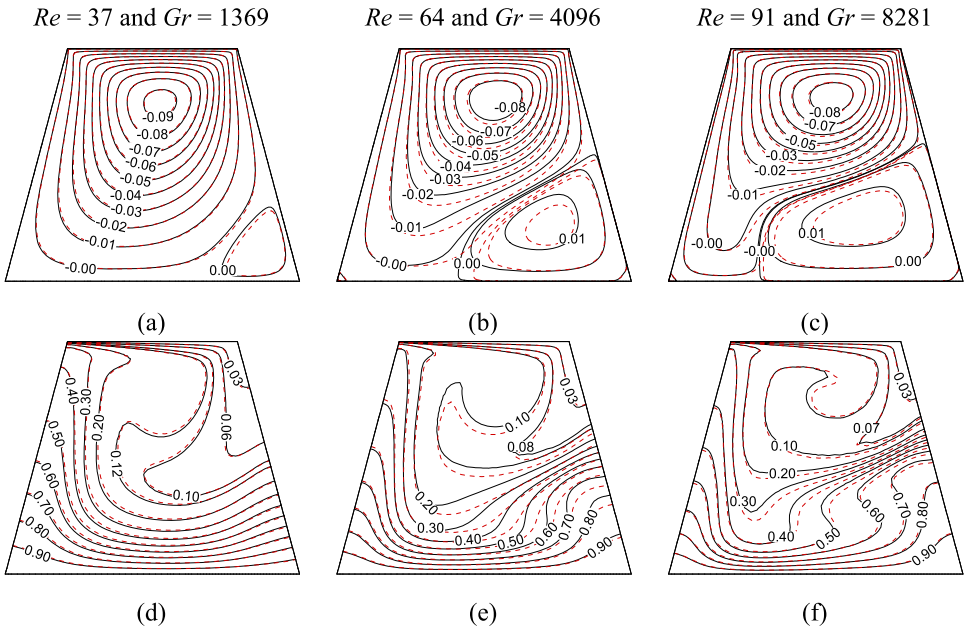

Fig. 15. Plots of (a)-(c) streamlines and (d)-(f) isotherms between nanofluid and plain fluid for different values of Re and Gr at $\theta = 0°$, $Ri = 1$ inside longer base trapezoidal enclosure. The solid lines (—) represent data for plain fluid, whereas the dotted lines (- - - -) represent the same for nanofluid.

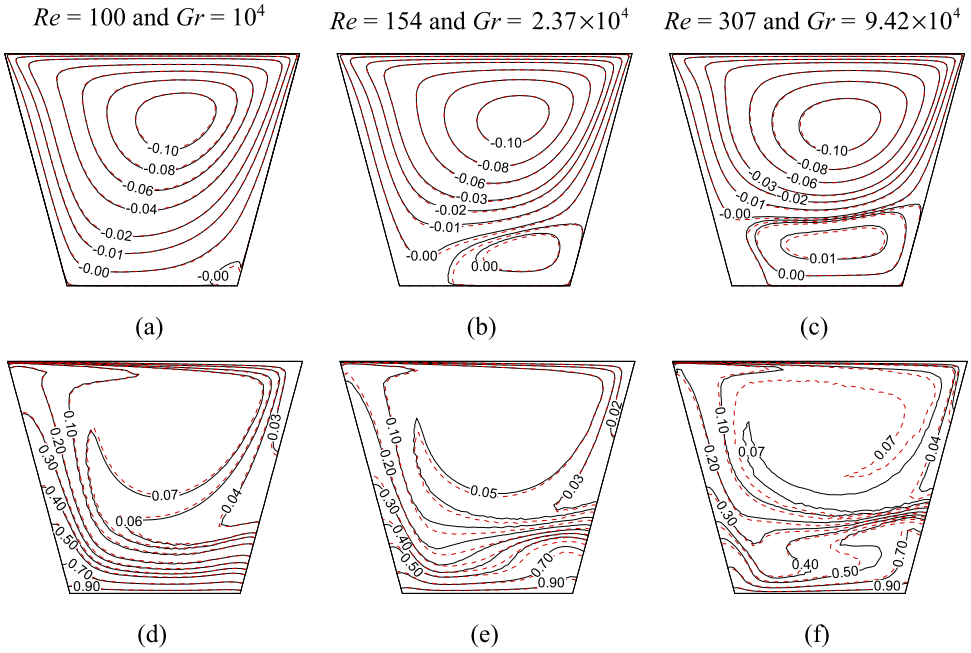

Fig. 16. Plots of (a)-(c) streamlines and (d)-(f) isotherms between nanofluid and plain fluid for different values of Re and Gr at $\theta = 0°$, $Ri = 1$ inside shorter base trapezoidal enclosure. The solid lines (—) represent data for plain fluid, whereas the dotted lines (- - - -) represent the same for nanofluid.

Three key aspects are highlighted in this figure. At first, conduction to convection transition is seen in the laminar zone. This is because the average Nusselt number stays unchanged at lower Reynolds number up to $Re = 3$ and $Gr = 9$ for both types of enclosure. After that, another transition is observed when the average Nusselt number drops suddenly and then gradually increases with increasing Re and Gr. It is caused by the shift from laminar to chaotic state. Another important observation can be seen that both Reynolds and Grashof numbers, at which laminar to chaotic transition takes place, decrease with an increase of bottom wall tilt angle. Besides, these critical Re and Gr are lower for the longer base trapezoid that shorter base trapezoid.

Two correlations of average Nusselt number of the heated wall are proposed for longer and shorter base trapezoids based on the outcomes of pure mixed convection (case 3) at $\phi = 1\%$. To eliminate dimensionality associated with the tilt angle, it is divided by 90° in the proposed correlations (20)–(21). The R^2 values for those correlations are 0.9948 and 0.9853 respectively. Theoretical support for related engineering applications may be provided by these correlations. The correlations can be expressed in the following way:

For longer base trapezoid:

$$Nu = 1.1505 - 0.5636\left(\frac{\theta}{90}\right)^{0.0105} + 0.0939Re^{0.7242}; \quad 0° \le \theta \le 45°,\ 0.1 \le Re \le 10^3, \tag{20}$$

For shorter base trapezoid:

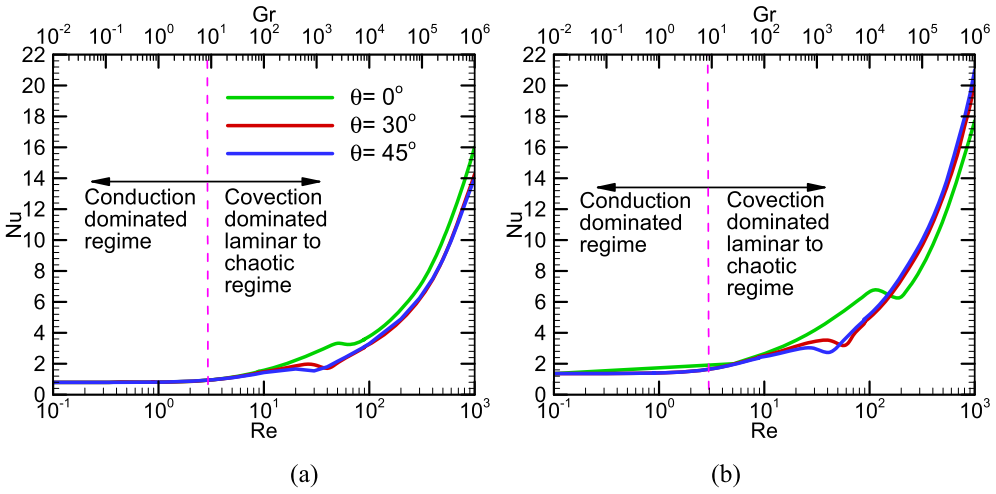

Fig. 17. Variation of average Nusselt number of the heated base wall of (a) longer base trapezoid and (b) shorter base trapezoid with Reynolds and Grashof numbers for different tilt angles at $Ri = 1$ and $\phi = 1\%$.

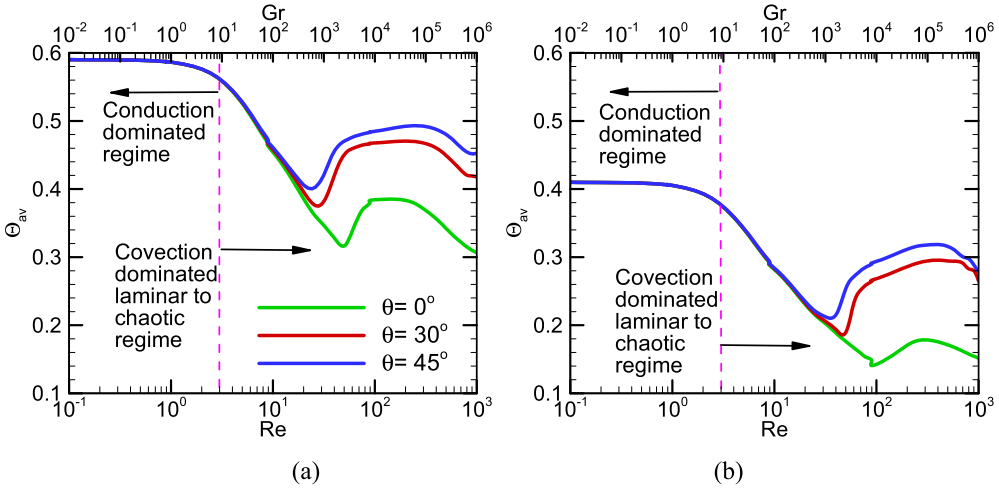

Fig. 18. Variation of average fluid temperature of (a) longer base trapezoid and (b) shorter base trapezoid with Reynolds and Grashof numbers for different tilt angles at $Ri = 1$ and $\phi = 1\%$.

$$Nu = 1.3473 + 3.6574\left(\frac{\theta}{90}\right)^{4.7762} + 0.1848Re^{0.6619};$$
$$0° \le \theta \le 45°,\ 0.1 \le Re \le 10^3. \quad (21)$$

Figs. 18(a)-(b) present the variation of average fluid temperature in both types of enclosure with simultaneous change of Reynolds and Grashof numbers for different tilt angles at $Ri = 1$ and $\phi = 1\%$. Like Nu plots as shown in Fig. 17, there are three separate regimes. No change in average fluid temperature occurs when conduction is the dominant mode of heat transfer. In a laminar regime dominated by convection, the average fluid temperature decreases for both configurations. However, there is no difference of Θ_{av} with the change of base wall tilt angle until it reaches to the critical Re and Gr. Both enclosures exhibit significant variation of average fluid temperature after that transition regime. It is noticed that the average fluid temperature in an inclined enclosure is greater than that for a horizontal enclosure.

To observe the effect of entropy generation due to heat transfer, variation of average Bejan number with Re and Gr as a function of tilt angles is plotted in Figs. 19(a)-(b). Initially, total entropy generation is constant which indicates conduction dominated mode. Then, it is increasing with increasing Re and Gr. In the conduction dominated region, total entropy generates due to only viscosity of the fluid. As both Re and Gr increases, entropy generation due to heat transfer starts to form. Because increasing Re and Gr enhances heat transfer and movement of fluid inside the enclosure. Furthermore, an important observation can be seen that both trapezoids develop similar patterns of entropy generation for all tilt angles.

5. Conclusion

The steady entropy generation and mixed convective flow of nanofluid within an inclined lid-driven trapezoidal enclosure have been investigated numerically. The Reynolds, Grashof, and Richardson numbers, the tilt angle of the base wall, and the nanoparticle volume fraction are the primary parameters of interest in the present study. The following conclusions can be derived from the findings of this investigation:

- Both heat transmission and flow properties inside the enclosure are significantly influenced by the change of Richardson number. Up to a certain Richardson number, Nusselt number decreases, but after that, it increases gradually when Reynolds number is fixed. Besides, when Grashof number is fixed, Nusselt number decreases with increasing Richardson number and decreasing Reynolds number.
- The shorter base trapezoid transmits more heat than the longer base trapezoid (maximum increment in Nusselt number is almost 100%). However, entropy production patterns are nearly identical

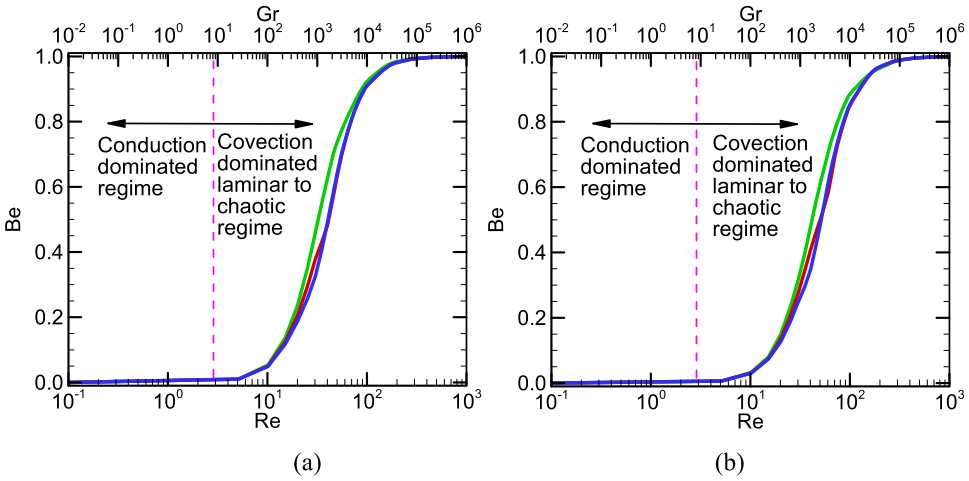

Fig. 19. Variation of average Bejan number of (a) longer base trapezoid and (b) shorter base trapezoid with Reynolds and Grashof numbers for different tilt angles at $Ri = 1$ and $\phi = 1\%$.

in both arrangements. The heat transfer performance deteriorates as the tilt angle of the base wall increases, yet the fluid temperature rises. During cases 1 and 2, the growth of entropy for heat transfer is far more dominant than the development of entropy due to viscosity.

- At a lower Reynolds number, changes from conduction to convection are seen in the laminar region for pure mixed convection ($Ri = 1$). For a longer base trapezoid, the Reynolds number at which the flow changes from laminar to chaotic is lower than for a shorter base trapezoid. Also, as the bottom wall tilt angle goes up, the Reynolds number at which the flow changes from laminar to chaotic drops.
- The average Nusselt number indicates the amount of heat transferred which is increased by the presence of nanofluid (the maximum increment is 29% for case 3 and longer base trapezoid). When the enclosure is filled with nanofluid, both the average fluid temperature and the average Bejan number decrease slightly.

Various aspects of the current inquiry have not been completely investigated due to various restrictions. In future investigations, the impacts and circumstances that described below can be used:

- Incorporation of the applied inclined magnetic field strength.
- Conjugate heat transfer with thick solid walls.
- Different cavity shapes, such as hexagonal, domed, triangular, etc., as well as various types of working fluids, notably conducting fluids such as hybrid nanofluids, phase change materials, etc.

Declarations

Author contribution statement

Md. Shahneoug Shuvo: Performed the experiments; Analyzed and interpreted the data; Contributed reagents, materials, analysis tools or data; Wrote the paper.

Mahmudul Hasan Hasib: Performed the experiments; Analyzed and interpreted the data; Wrote the paper.

Sumon Saha: Conceived and designed the experiments; Performed the experiments; Analyzed and interpreted the data; Contributed reagents, materials, analysis tools or data; Wrote the paper.

Funding statement

This research did not receive any specific grant from funding agencies in the public, commercial, or not-for-profit sectors.

Data availability statement

Data will be made available on request.

Declaration of interests statement

The authors declare no competing interests.

Additional information

No additional information is available for this paper.

Acknowledgements

Our heartiest gratitude is to the CFDHT Research Group of Department of Mechanical Engineering of BUET, Bangladesh for all sorts of guidance and support.

References

[1] R. Schreiber, H.B. Keller, Driven cavity flows by efficient numerical techniques, J. Comput. Phys. 49 (2) (1983 Feb 1) 310–333.
[2] M.C. Thompson, J.H. Ferziger, An adaptive multigrid technique for the incompressible Navier-Stokes equations, J. Comput. Phys. 82 (1) (1989 May 1) 94–121.
[3] N. Alleborn, H. Raszillier, F. Durst, N. Alleborn, H. Raszillier, F. Durst, Lid-driven cavity with heat and mass transport, Int. J. Heat Mass Transf. 42 (5) (1999 Mar 1) 833–853.
[4] K.M. Khanafer, J. Chamkha, Mixed convection flow in a lid-driven enclosure filled with a fluid-saturated porous medium, Int. J. Heat Mass Transf. 42 (13) (1999 Jul 1) 2465–2481.
[5] W.J. Yang, O. Aydin, Mixed convection in cavities with a locally heated lower wall and moving sidewalls, Numer. Heat Transf., Part A, Appl. 37 (7) (2000 Jun 12) 695–710.
[6] T. Javed, Z. Mehmood, I. Pop, MHD-mixed convection flow in a lid-driven trapezoidal cavity under uniformly/non-uniformly heated bottom wall, Int. J. Numer. Methods Heat Fluid Flow 27 (6) (2017 Jun 5) 1231–1248.
[7] N.A. Bakar, R. Roslan, A. Karimipour, I. Hashim, Mixed convection in lid-driven cavity with inclined magnetic field, Sains Malays. 48 (2) (2019 Feb 1) 451–471.
[8] P.Y. Xiong, A. Hamid, K. Iqbal, M. Irfan, M. Khan, Numerical simulation of mixed convection flow and heat transfer in the lid-driven triangular cavity with different obstacle configurations, Int. Commun. Heat Mass Transf. 123 (2021 Apr 1) 105202.
[9] Y. Xuan, Q. Li, Investigation on convective heat transfer and flow features of nanofluids, J. Heat Transf. 125 (1) (2003 Feb 1) 151–155.
[10] S.U.S. Choi, J.A. Eastman, Enhancing Thermal Conductivity of Fluids with Nanoparticles, Argonne National Lab. (ANL), Argonne, IL (United States), 1995 Oct 1.
[11] F. Talebi, A.H. Mahmoudi, M. Shahi, Numerical study of mixed convection flows in a square lid-driven cavity utilizing nanofluid, Int. Commun. Heat Mass Transf. 37 (1) (2010 Jan 1) 79–90.
[12] M. Mahmoodi, Mixed convection inside nanofluid filled rectangular enclosures with moving bottom wall, Therm. Sci. 15 (3) (2011) 889–903.

[13] M.A. Mansour, R.A. Mohamed, M.M. Abd-Elaziz, S.E. Ahmed, Numerical simulation of mixed convection flows in a square lid-driven cavity partially heated from below using nanofluid, Int. Commun. Heat Mass Transf. 37 (10) (2010 Dec 1) 1504–1512.
[14] M.M. Rahman, M.M. Billah, A.T.M.M. Rahman, M.A. Kalam, A. Ahsan, Numerical investigation of heat transfer enhancement of nanofluids in an inclined lid-driven triangular enclosure, Int. Commun. Heat Mass Transf. 38 (10) (2011 Dec 1) 1360–1367.
[15] M.A. Ismael, T. Armaghani, A.J. Chamkha, Mixed convection and entropy generation in a lid-driven cavity filled with a hybrid nanofluid and heated by a triangular solid, Heat Transf. Res. 49 (17) (2018) 1645–1665.
[16] I.R. Ali, Al. Alsabery, N.A. Bakar, R. Roslan, Mixed convection in a double lid-driven cavity filled with hybrid nanofluid by using finite volume method, Symmetry 12 (12) (2020 Nov 30) 1977, 1–15.
[17] M.A.H. Mamun, T.R. Tanim, M.M. Rahman, R. Saidur, S. Nagata, Mixed convection analysis in trapezoidal cavity with a moving lid, Int. J. Mech. Mater. Eng. 5 (1) (2010) 18–28.
[18] M. Bhattacharya, T. Basak, H.F. Oztop, Y. Varol, Mixed convection and role of multiple solutions in lid-driven trapezoidal enclosures, Int. J. Heat Mass Transf. 63 (2013 Aug 1) 366–388.
[19] M.H. Hasib, M.S. Hossen, S. Saha, Effect of tilt angle on pure mixed convection flow in trapezoidal cavities filled with water-Al_2O_3 nanofluid, Proc. Eng. 105 (2015) 3897.
[20] A. Aghaei, H. Khorasanizadeh, G. Sheikhzadeh, M. Abbaszadeh, Numerical study of magnetic field on mixed convection and entropy generation of nanofluid in a trapezoidal enclosure, J. Magn. Magn. Mater. 403 (2016 Apr 1) 133–145.
[21] A.K. Kareem, H.A. Mohammed, A.K. Hussein, S. Gao, Numerical investigation of mixed convection heat transfer of nanofluids in a lid-driven trapezoidal cavity, Int. Commun. Heat Mass Transf. 77 (2016 Oct 1) 195–205.
[22] A. Arefmanesh, A. Aghaei, H. Ehteram, Mixed convection heat transfer in a CuO–water filled trapezoidal enclosure, effects of various constant and variable properties of the nanofluid, Appl. Math. Model. 40 (2) (2016 Jan 15) 815–831.
[23] F. Selimefendigil, H.F. Öztop, A.J. Chamkha, Analysis of mixed convection of nanofluid in a 3D lid-driven trapezoidal cavity with flexible side surfaces and inner cylinder, Int. Commun. Heat Mass Transf. 87 (2017 Oct 1) 40–51.
[24] F. Selimefendigil, H.F. Öztop, Modeling and optimization of MHD mixed convection in a lid-driven trapezoidal cavity filled with alumina–water nanofluid: effects of electrical conductivity models, Int. J. Mech. Sci. 136 (2018 Feb 1) 264–278.
[25] D. Toghraie, Numerical simulation on MHD mixed convection of Cu-water nanofluid in a trapezoidal lid-driven cavity, Int. J. Appl. Electromagn. Mech. 62 (4) (2020 Jan 1) 683–710.
[26] W. Ibrahim, M. Hirpho, Finite element analysis of mixed convection flow in a trapezoidal cavity with non-uniform temperature, Heliyon 7 (1) (2021 Jan 1) e05933.
[27] S.S. Shah, R.U. Haq, W. Al-Kouz, Mixed convection analysis in a split lid-driven trapezoidal cavity having elliptic shaped obstacle, Int. Commun. Heat Mass Transf. 126 (2021 Jul 1) 105448.
[28] P. Mondal, T.R. Mahapatra, MHD double-diffusive mixed convection and entropy generation of nanofluid in a trapezoidal cavity, Int. J. Mech. Sci. 208 (2021 Oct 15) 106665.
[29] M.S. Ishak, A.I. Alsabery, I. Hashim, A.J. Chamkha, Entropy production and mixed convection within trapezoidal cavity having nanofluids and localised solid cylinder, Sci. Rep. 11 (1) (2021 Jul 19) 1–22.
[30] S. Izadi, T. Armaghani, R. Ghasemiasl, A.J. Chamkha, M. Molana, A comprehensive review on mixed convection of nanofluids in various shapes of enclosures, Powder Technol. 343 (2019 Feb 1) 880–907.
[31] M.A. Mustafa, H.M. Hussain, A.A. Abtan, L.J. Habeeb, Review on mixed convective heat transfer in different geometries of cavity with lid driven, J. Mech. Eng. Res. Dev. 43 (7) (2020) 12–25.
[32] W.H. Azmi, K.V. Sharma, R. Mamat, G. Najafi, M.S. Mohamad, The enhancement of effective thermal conductivity and effective dynamic viscosity of nanofluids–a review, Renew. Sustain. Energy Rev. 53 (2016 Jan 1) 1046–1058.
[33] O.C. Zienkiewicz, R.L. Taylor, The Finite Element Method, Volume 1 The Basis, Wiley, 2000, pp. 128–132.
[34] M. Roy, T. Basak, S. Roy, I. Pop, Analysis of entropy generation for mixed convection in a square cavity for various thermal boundary conditions, Numer. Heat Transf., Part A, Appl. 68 (1) (2015 Jul 3) 44–74.
[35] R. Iwatsu, J.M. Hyun, K. Kuwahara, Mixed convection in a driven cavity with a stable vertical temperature gradient, Int. J. Heat Mass Transf. 36 (6) (1993 Jan 1) 1601–1608.
[36] A.M. Al-Amiri, Analysis of momentum and energy transfer in a lid-driven cavity filled with a porous medium, Int. J. Heat Mass Transf. 43 (19) (2000 Oct 1) 3513–3527.